Chemistry–A European Journal
Research Article
doi.org/10.1002/chem.202200974
Chemistry Europe
European Chemical Societies Publishing
www.chemeurj.org

Electrochemistry and Reactivity of Chelation-stabilized Hypervalent Bromine(III) Compounds

Nayereh Mohebbati,[a, b] Igors Sokolovs,[c] Philipp Woite,[d] Märt Lõkov,[e] Elisabeth Parman,[e] Mihkel Ugandi,[d] Ivo Leito,*[e] Michael Roemelt,*[d] Edgars Suna,*[c, f] and Robert Francke*[a, b]

Abstract: Hypervalent bromine(III) reagents possess a higher electrophilicity and a stronger oxidizing power compared to their iodine(III) counterparts. Despite the superior reactivity, bromine(III) reagents have a reputation of hard-to-control and difficult-to-synthesize compounds. This is partly due to their low stability, and partly because their synthesis typically relies on the use of the toxic and highly reactive BrF_3 as a precursor. Recently, we proposed chelation-stabilized hypervalent bromine(III) compounds as a possible solution to both problems. First, they can be conveniently prepared by electro-oxidation of the corresponding bromoarenes. Second, the chelation endows bromine(III) species with increased stability while retaining sufficient reactivity, comparable to that of iodine(III) counterparts. Finally, their intrinsic reactivity can be unlocked in the presence of acids. Herein, an in-depth mechanistic study of both the electrochemical generation and the reactivity of the bromine(III) compounds is disclosed, with implications for known applications and future developments in the field.

Introduction

The chemistry of hypervalent halogen species has experienced tremendous progress in recent decades, with hypervalent iodine(III) compounds playing an increasingly important role in modern organic synthesis.[1] The related isoelectronic hypervalent bromine(III) reagents exhibit stronger electrophilicity, better nucleofugality of the bromanyl unit, and more driving force for oxidations,[2–4] as evidenced by a series of unprecedented synthetic transformations involving oxidative coupling of alkynes and primary alcohols to conjugated enones,[5] Hofmann rearrangement of sulfonamides to the corresponding *N*-arylsulfamoyl fluorides,[6] regioselective C–H functionalization of non-activated alkanes,[7,8a] and a rare Bayer-Villiger-type oxidation of open-chain aliphatic aldehydes.[9] Recently, the application of diaryl-λ^3-bromanes in catalysis[10] and in cycloaddition reactions[11] was also reported. Although these notable achievements underscore the remarkable synthetic potential of this reagent class, hypervalent bromine(III) chemistry appears to be underdeveloped in comparison to that of the iodine(III) counterparts. This notable disparity has been ascribed to two unfavorable factors. First, bromine(III) reagents exhibit poor stability and high oxidizing power, which has led to the general perception of difficult-to-control reactivity and poor compatibility with functional groups.[2,3] Second, conventional routes to λ^3-bromane reagents rely eventually on the use of BrF_3, a highly toxic and extremely reactive liquid that demands for specific equipment and experimental techniques for its safe handling.[8]

Recently, a chelation-stabilized λ^3-bromane reagent[12] (Martin's bromane **2**, Scheme 1) was proposed as a possible solution to both the stability and the accessibility issue. Inspired by the successful *in situ* generation of reactive hypervalent iodine species via anodic oxidation of iodoarene precursors,[13,14] we presented a convenient electrochemical approach toward synthesis of **2**.[15] The method is based on the anodic oxidation of parent aryl bromides **1** containing two coordinating hexafluoro-2-hydroxy-propanyl substituents under galvanostatic conditions in an undivided cell (Eq. (1) in Scheme 1). The protocol was used to prepare a series of *para*-substituted derivatives of

[a] *N. Mohebbati, Prof. Dr. R. Francke*
Leibniz Institute for Catalysis
Albert-Einstein-Str. 29a, 18059 Rostock (Germany)
E-mail: robert.francke@catalysis.de
[b] *N. Mohebbati, Prof. Dr. R. Francke*
Institute of Chemistry
Rostock University
Albert-Einstein-Str. 3a, 18059 Rostock (Germany)
[c] *Dr. I. Sokolovs, Prof. Dr. E. Suna*
Latvian Institute of Organic Synthesis
Aizkraukles 21, 1006 Riga (Latvia)
E-mail: edgars@osi.lv
[d] *P. Woite, M. Ugandi, Prof. Dr. M. Roemelt*
Department of Chemistry
Humboldt-University of Berlin
Brook-Taylor-Str. 2, 12489 Berlin (Germany)
E-mail: michael.roemelt@hu-berlin.de
[e] *Dr. M. Lõkov, E. Parman, Prof. Dr. I. Leito*
Institute of Chemistry
University of Tartu
Ravila 14a, 50411 Tartu (Estonia)
E-mail: ivo.leito@ut.ee
[f] *Prof. Dr. E. Suna*
Faculty of Chemistry
University of Latvia
Jelgavas 1, 1004 Riga (Latvia)

Supporting information for this article is available on the WWW under https://doi.org/10.1002/chem.202200974

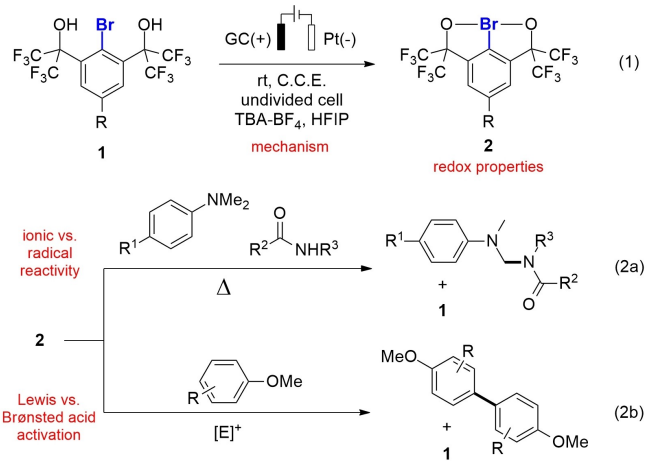

Scheme 1. Electrochemical generation of aryl-λ^3-bromanes **2** (Eq. (1)) and applications as reagent (Eq. (2)).

Martin's bromane **2** that revealed remarkably high redox potentials covering a range from 1.86 V to 2.60 V versus Ag/$AgNO_3$. The compounds are benchtop-stable and have proven useful as reagents in various transformations. Thus, λ^3-bromane **2a** (R=H) was shown to be sufficiently reactive to effect clean oxidative amidation of aniline derivatives (Eq. (2a) in Scheme 1). Furthermore, the intrinsic reactivity of hypervalent bromine(III) species can be unlocked by addition of Brønsted or Lewis acids, for example to achieve dehydrogenative homocoupling of substituted anisoles (Eq. (2b) in Scheme 1). Herein, mechanistic insights into both the electrochemical generation and the reactivity of chelation-stabilized bromine(III) compounds are disclosed.

Results and Discussion

Anodic bromane generation

To better understand the mechanism of bromane formation, we intended to combine detailed electroanalytical studies with quantum chemical modeling. In our previous work,[15] we have already obtained some information about bromoarene oxidation by performing preliminary electroanalytical experiments. Thus, voltammetric analysis of **1** at 10 mV s^{-1} between 0 and 2.7 V versus Ag/0.01 M $AgNO_3$ (E_{ref} = −87 mV vs. Fc/Fc^+ couple)[16] using an electrolyte consisting of 0.1 M NBu_4BF_4 in HFIP showed that each of the bromoarenes exhibits a single irreversible anodic feature. The corresponding half-peak potentials ($E_{P/2}$) are situated between 1.86 V (**1e**, R=OMe) and 2.60 V (**1g**, R=NO_2), which means that the potential of **1** is flexibly tunable within a range of 0.74 V (see Table 1). A linear relationship between $E_{p/2}$ and σ_P^+ substituent coefficients showed that the oxidizability is dependent on the electron donating or withdrawing ability of the substituent R and that the redox potential of the **1**/**2** couple thus exhibits a somewhat predictable behavior.

Table 1. Summary of the half-peak potentials ($E_{P/2}$, determined at v = 10 mV s^{-1}) and slopes of the j_p vs. $v^{0.5}$ plots for the anodic oxidation of **1** in HFIP.

compound	R	$E_{P/2}$ [V]	slope j_p vs. $v^{0.5}$ [mA $s^{0.5}$ $mV^{-0.5}$ cm^{-2}]
1a	H	2.27	0.156
1b	F	2.26	0.161
1c	Cl	2.22	0.194
1d	*t*Bu	2.13	0.168
1e	OMe	1.86	0.088
1f	CF_3	2.54	0.150
1g	NO_2	2.60	0.140

For the present study, one of the aims was to learn more about the mechanism of the formation of **2**. For this purpose, the scan rate v was increased stepwise from 10 mV s^{-1} to 1 V s^{-1}. The observed voltammetric responses of **1a** are characteristic for the bromoarene series with the signal shape indicating that one or more chemical steps are coupled to the electron transfer ("chemical irreversibility", see representative CVs in Figure 1A).[17] Bromoarenes **1b–d**, **1f** and **1g** exhibit analogous behavior (see the Supporting Information), whereas the voltammetry of **1e** (R=OMe) is rather exceptional (Figure 1B). Initially, **1e** displays irreversible behavior at low scan rates (dashed curve), followed by a gradual change to almost full reversibility with increasing v (dotted and solid lines, for $j_{p,ox}/j_{p,red}$ ratios see Table S2 in the Supporting Information),

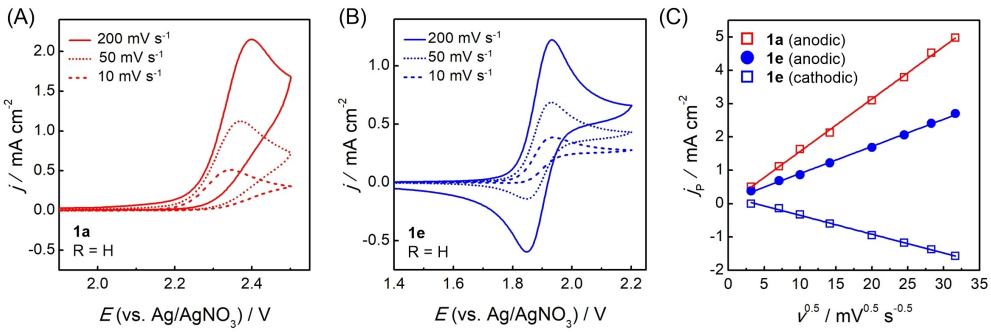

Figure 1. A and B: Background and *iR* drop-corrected CVs of 5 mM **1a** and 5 mM **1e** at different scan rates (solvent: HFIP, working electrode: glassy carbon, supporting electrolyte: 0.1 M Bu_4NBF_4). C: Plot of the peak current densities (j_P) vs. $v^{0.5}$.

indicating that the intermediate formed upon electron transfer is stable on the voltammetry time scale.

Another striking difference between **1e** and the other bromoarenes is that the anodic peak current density j_p of the 4-OMe-substituted compound is significantly smaller. Both j_P and the slope of the linear fit of j_p versus $v^{0.5}$ are approximately half as high as the average values for the other compounds (see Figure 1C and Table 1). One-electron oxidation of **1e** and two-electron oxidation of the other bromoarenes, provide a reasonable rationale for this difference. In fact, it is well-established that a j_p value (and a j_p vs. $v^{0.5}$ slope, respectively) twice as high as for a comparable one-electron transfer is characteristic of a two-electron process in which *i*), the second oxidation is energetically more favorable than the first one and *ii*), in which a fast chemical reaction is interposed between the two electrochemical steps.[18]

A mechanism consistent with the observations described above is shown in Figure 2. Accordingly, bromanes **2** are generally formed via two electrochemical oxidation steps in an ECEC pathway, which includes initial electron abstraction, deprotonation, further oxidation, and a second deprotonation (leading to $\mathbf{1}^{\bullet+}$, $\mathbf{1}^{\bullet}$, $\mathbf{2}^{+}$, and **2**, respectively). Competitive homogeneous disproportionation of $\mathbf{1}^{\bullet}$ (or between $\mathbf{1}^{\bullet+}$ and $\mathbf{1}^{\bullet}$) within the diffusion layer would also be in agreement with the diagnostic criteria (ECE_{disp} pathway).[17] However, when the deprotonation step $\mathbf{1}^{\bullet+}\rightarrow\mathbf{1}^{\bullet}$ is slow due to a stabilization of $\mathbf{1}^{\bullet+}$,

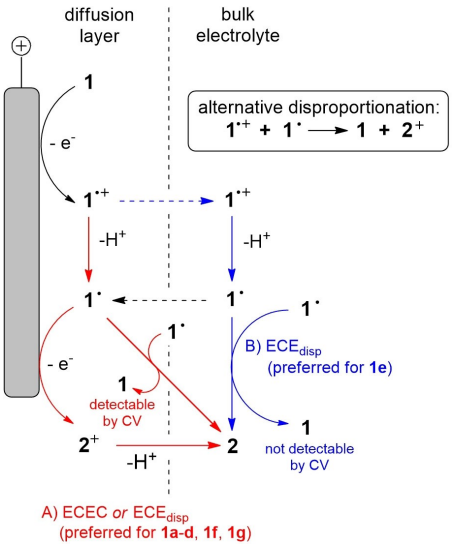

Figure 2. Proposed mechanism for anodic bromane formation.

the radical cation has sufficient time to diffuse into the bulk solution, where $\mathbf{1}^{\bullet}$ is slowly formed (Figure 2, pathway highlighted in blue). Subsequent disproportionation again leads to the formation of **2** and **1** ($\mathbf{2}^{+}$ and **1**, respectively). Such a delayed disproportionation would explain the distinct behavior of **1e**, as it is in agreement both with the one electron peak in the CV and the observed formation of **2e** in the preparative-scale electrolysis. Here, the electron-donating ability of the 4-methoxy substituent seems to be responsible for the enhancement of the lifetime of $\mathbf{1e}^{\bullet+}$.

Further probing into the mechanism of bromane formation was carried out with a series of quantum chemical calculations using a state-of-the-art combination of density functional theory and coupled cluster methods (see computational details in the Supporting Information). The obtained results presented in Table 2 confirm the feasibility of the reaction sequence $\mathbf{1}\rightarrow\mathbf{1}^{\bullet+}\rightarrow\mathbf{1}^{\bullet}\rightarrow\mathbf{2}^{+}\rightarrow\mathbf{2}$ in terms of reaction free energies for all investigated derivatives. For all proton transfer reactions, cathodically generated HFIP anions have been assumed as proton acceptors, as has been established previously.[14] The investigated deprotonations occur spontaneously without any barrier *in silico*. Similarly, the outer sphere electron transfer is expected to be associated with reaction barriers that are readily overcome under the given reaction conditions, since the redox-active sites are well accessible in all cases.

A closer look at the individual reaction steps yields interesting insight into certain aspects of the observed reactivity and provides further support for the proposed reaction mechanism (Table 2). For example, in good agreement with the experimental observations, the calculated ionization energy of $\mathbf{1}^{\bullet}$ is lower than that of **1**, rendering the second electron transfer more favorable than the first one. In contrast, the ionization free energy of $\mathbf{1}^{\bullet+}$ is predicted to be significantly higher. On the basis of these results, the possibility for formation of **2** via an EEC mechanism appears unlikely.

It is furthermore interesting to consider the calculated free energy of the disproportionation reactions $\mathbf{1}^{\bullet+}+\mathbf{1}^{\bullet}\rightarrow\mathbf{2}+\mathbf{2}^{+}$ as well as $2\ \mathbf{1}^{\bullet}\rightarrow\mathbf{1}+\mathbf{2}$, which are favorable for all investigated derivatives with predicted free energies of approx. $-30\ kcal\,mol^{-1}$. Only for $\mathbf{1e}^{\bullet+}+\mathbf{1e}^{\bullet}\rightarrow\mathbf{2e}+\mathbf{2e}^{+}$ the reaction free energy is significantly less negative ($-14.5\ kcal\,mol^{-1}$). This finding can be attributed to the relative stability of $\mathbf{1e}^{\bullet+}$ that originates from the electron-donating character of the 4-methoxy group. The spin density plots shown in Figure 3 reflect this assessment. Moreover, our calculations indicate that $\mathbf{1e}^{+\bullet}$ is less prone to deprotonation than all other $\mathbf{1}^{+\bullet}$ derivatives ($-34.0\ kcal\,mol^{-1}$ vs. approx. $-50\ kcal\,mol^{-1}$) and thereby cor-

Table 2. Calculated [DFT + DLPNO-CCSD(T)] reaction free energies (in kcal mol^{-1}) for all elementary steps of the electrochemical conversion of **1** to **2**.

Derivative	$1\rightarrow1^{\bullet+}$	$1^{\bullet+}\rightarrow1^{\bullet}$	$1^{\bullet+}\rightarrow1^{2+}$	$1^{\bullet}\rightarrow2^{+}$	$2^{+}\rightarrow2$	$1\rightarrow2$	$2\ 1^{\bullet}\rightarrow1+2$	$1^{\bullet+}+1^{\bullet}\rightarrow2+2^{+}$
a	169.9	−49.2	180.3	139.2	−49.5	210.5	−31.1	−30.7
b	170.8	−49.8	181.4	141.4	−50.1	212.4	−29.6	−29.4
c	170.4	−49.4	180.8	141.8	−51.3	211.5	−30.5	−28.6
d	169.0	−48.0	178.9	139.7	−49.1	211.6	−30.3	−29.3
e	154.5	−34.0	169.6	140.0	−50.0	210.5	−30.5	−14.5
f	170.9	−50.5	180.5	143.0	−52.7	210.7	−30.1	−28.0
g	171.5	−51.3	182.2	143.5	−52.3	211.4	−29.1	−28.1

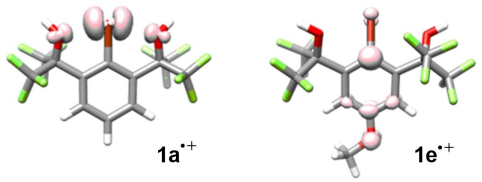

Figure 3. Comparison between the spin density distributions of **1a**$^{\bullet+}$ and **1e**$^{\bullet+}$.

roborate the proposed mechanism for the formation of **2e**. Considering the significant driving force for both disproportionation reactions, we assume that the predominant reaction type will most likely be determined by the availability of the involved species (**1e**$^{\bullet+}$ vs. **1e**$^{\bullet}$) rather than by thermodynamic factors.

Another experimental observation supports the proposed ECE_{disp} mechanism for **1e**→**2e**. During preparative-scale electrolysis of **1**, the electrolyte solution usually remains colorless or, sometimes, becomes slightly yellowish. Only the oxidation of **1e** leads to a deep red coloration of the electrolyte solution, which disappears shortly after switching off the current. This prompted us to perform a spectroelectrochemical (SEC) analysis of the oxidation of **1e** (see Figure 4). After applying a potential of 2.0 V, two bands arise simultaneously at 336 nm and 534 nm (Figure 4, bottom) in addition to the band of **1e** at 288 nm. An apparent increase of the latter can be assigned to formation of **2e**, which absorbs at similar wavelengths (284 nm, see pure component spectrum in Figure 4, top). The new features are in good agreement with the bands predicted by quantum chemical calculations (321 nm and 487 nm). Noteworthy, no bands in the respective energy regimes are predicted for **1e**$^{\bullet}$ and **2e**$^{+}$ (see Table S8 in the Supporting Information). After switching off the potential, the bands at 336 nm and 534 nm rapidly disappear, while the signal for **2e** continues to increase, which is further evidence for the proposed disproportionation mechanism.

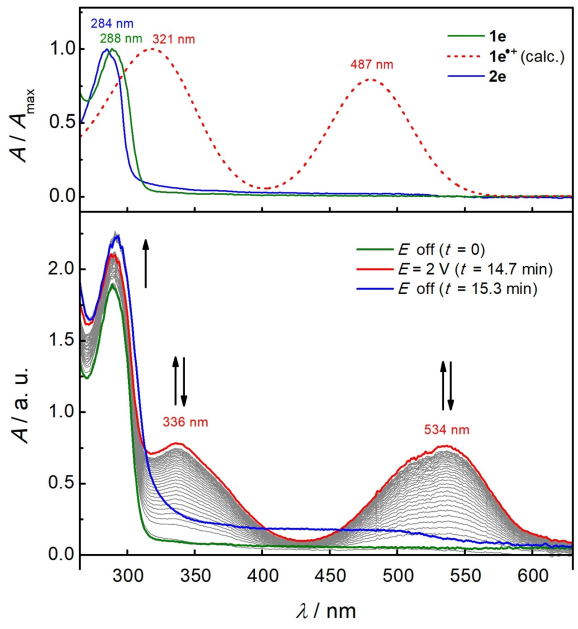

Figure 4. Top: Absorption spectra of pure **1e** (green line) and **2e** (blue line) recorded in HFIP along with the predicted spectrum of **1e**$^{\bullet+}$ (dotted red line). Bottom: Spectroelectrochemical analysis of the anodic oxidation of **1e** at $E = 2.0$ V vs. $Ag/AgNO_3$ (anode: Pt grid).

Cathodic reduction of bromanes

As described in the previous section, the CVs of the bromoarenes recorded in HFIP show that with the exception of **1e**, the compounds are irreversibly oxidized, meaning that there is no associated reduction peak in the reverse scan. Thus, the anodically generated bromanes appear to be surprisingly robust toward reduction at the cathode. Knowledge of the cathodic behavior is still desirable, as it allows conclusions to be drawn about the properties of **2** as a chemical oxidant (see below). In this regard, an electroanalytical study demands for employing solvents that were used in the synthetic applications, that is, acetonitrile for C–H amidations and dichloromethane for arene-arene homocouplings (Eq. (2a) and (2b) in Scheme 1).[15] CV studies of the cathodic reduction were thus carried out in each of these solvents using a glassy carbon working electrode and NBu_4BF_4 as the supporting electrolyte, whereby both the shape of the profiles and the half-peak potentials are quite similar.

In the range between 0.1 and −0.9 V, each of the bromanes exhibits a single irreversible feature, indicating that electron transfer is followed by a rapid chemical step. The forward scans are shown in Figure 5 exemplarily for acetonitrile (for full CVs, see the Supporting Information). The corresponding $E_{P/2}$ values are situated in the range between −0.35 V (**2g**, R=NO_2) and −0.53 V (**2e**, R=OMe; see table in Figure 5). It follows that *i*) electrochemical reduction of **2** is relatively difficult, *ii*) with 0.18 V, the range of reduction potentials covered by series **2** is relatively narrow compared to the range of oxidation potentials of **1** (0.74 V). A good match was found between the experimental half-peak potentials and $E_{P/2}$ values predicted on the basis of a two-parameter correlation with σ_F and σ_R substituent constants (Figure 5, bottom right; for details see Tables S5 and S6 in the Supporting Information), the latter two explicitly accounting for inductive (σ_F) and resonance effects (σ_R).[19] Accordingly, there is a correlation between $E_{P/2}$ and electron-donating/withdrawing ability of R, indicating the inclusion of the aromatic ring in the reduction process (albeit, apparently, to a much lesser extent than for the oxidation of **1**).

Surprisingly, further analysis of the reduction peaks shows that the process, both in CH_3CN and CH_2Cl_2, is associated with merely a single electron exchange (see the Supporting Information). To better understand the underlying mechanism, **2a** was subjected to controlled potential electrolysis (CPE, Scheme 2). In acetonitrile, bromoarene **1a** could be isolated in 74% yield after passing 1.0 F at −0.78 V versus Ag/0.01 M $AgNO_3$ (11% recovered **2a**). This result is in agreement with the one electron peak observed in the CV experiments, and can be explained by initial formation of radical anion **2a**$^{\bullet-}$, followed by

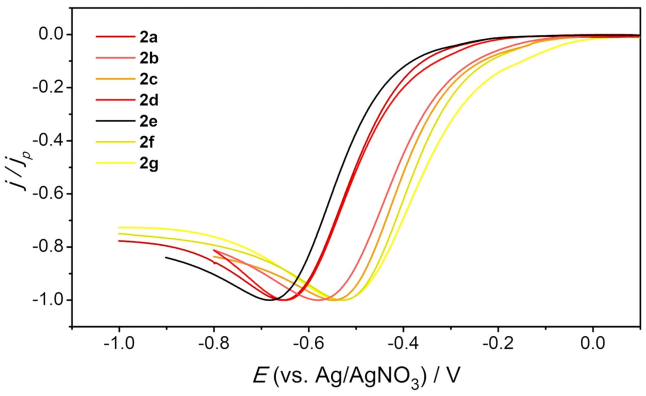

compound (group R)	$E_{P/2}$ (obs.) [V]	$E_{P/2}$ (pred.) [V]
2a (H)	-0.50	-0.50
2b (F)	-0.41	-0.42
2c (Cl)	-0.39	-0.43
2d (*t*-Bu)	-0.50	-0.50
2e (OMe)	-0.53	-0.50
2f (CF_3)	-0.37	-0.38
2g (NO_2)	-0.35	-0.33

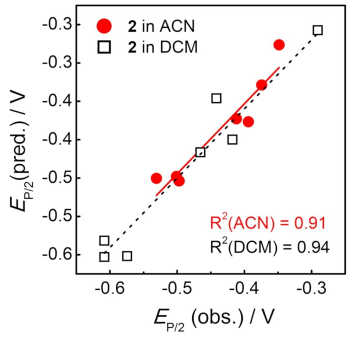

Figure 5. Top: Background and *iR* drop corrected linear sweep voltammograms (LSV) of bromanes **2a-g** (c = 5 mM) recorded at 10 mV s^{-1} in CH_3CN. Bottom left: Half-peak potentials $E_{P/2}$(obs.) measured in CH_3CN and the values predicted using σ_R and σ_F substituent constants ($E_{P/2}$(pred.), for details see the Supporting Information). Bottom right: Correlation between $E_{P/2}$(obs.) and $E_{P/2}$(pred.) for **2** in CH_2Cl_2 and CH_3CN.

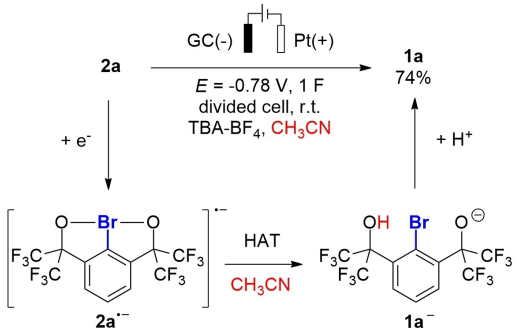

Scheme 2. Results of preparative-scale cathodic reduction of **2a** in CH_3CN.

hydrogen atom transfer (HAT) from a solvent molecule leading to $\mathbf{1a}^-$.[20] The latter is protonated either by anodically generated acids (the anodic half-cell reaction is electrolyte degradation)[21] or during workup.

Ionic versus radical reactivity

The results of the cathodic scans and CPE suggest that although formation of $\mathbf{2a}^{\bullet-}$ is in principle feasible, the one electron reduction is unfavorable and proceeds at negative potentials. For applications in synthetic organic chemistry, λ^3-bromane **2a** can thus be considered a poor single electron oxidant. This important finding prompted us to study mechanisms of the recently published reactions involving **2a**, such as oxidative amination of *N*,*N*-dimethylanilines **3** (Eq. (1), Scheme 3).[15] The oxidative amination apparently proceeds through the addition of phthalimide **5** to iminium ion **4a** that is formed *in situ* from parent aniline **3a** and hypervalent bromine(III) reagent **2a**. A calculated free energy of −19.3 kcal mol^{-1} confirms the thermodynamical feasibility of iminium **4a** formation induced by **2a**. However, a literature survey returns controversial mechanisms for iminium **4a** formation from aniline **3a** and hypervalent iodine(III) species, related to **2a**. Thus, a single electron transfer (SET) from aniline **3a** to hydroxybenziodoxole[22] or PIDA[23] was proposed to generate transient radical cation $\mathbf{3a}^{\bullet+}$ *en route* to the iminium ion **4a** (Eq. (2), Scheme 3). An alternative mechanistic scenario towards iminium ion **4a** involves β-deprotonation of transient aniline-containing iodine(III) species **TS-2** (Eq. (3), Scheme 3).[24] Given the apparent inconsistency in the mechanism of the iodine(III)-mediated oxidative amination reaction, we decided to examine in more detail the reaction of aniline **3a** with λ^3-bromane **2a**.

The comparison of the measured oxidation potential for aniline **3a** ($E_{P/2}$ = 0.40 V) with the reduction potential of λ^3-bromane **2a** ($E_{P/2}$ = −0.50 V) in MeCN shows a large potential gap of 0.9 V, suggesting that SET oxidation of aniline **3a** by **2a** is thermodynamically unfavorable. This assessment is supported by calculations showing that the formation of $\mathbf{2a}^{\bullet-}$ and $\mathbf{3a}^{\bullet+}$ is endergonic ($\triangle G$ = 20.1 kcal mol^{-1}). Of note, electrochemically generated radical cation $\mathbf{3a}^{\bullet+}$ was found to be highly unstable and short-lived in MeCN with a half-life on the order of microseconds.[25] Furthermore, radical cation $\mathbf{3a}^{\bullet+}$ was reported to undergo rapid dimerization to *N*,*N*,*N*,*N*-tetramethylbenzidene (TMB; see Scheme 2, Eq. (2)) with an extremely high rate constant ($k = 2.5 \times 10^8$ M^{-1} s^{-1}).[26] The lack of evidence for the formation of TMB upon mixing the equimolar amounts of **2a** and **3a** in MeCN (in absence of **5**) renders highly unlikely the involvement of radical cation $\mathbf{3a}^{\bullet+}$ in the oxidative amination.[27]

Additional experimental evidence against the intermediacy of radical cation $\mathbf{3a}^{\bullet+}$ in the oxidative amination was obtained by a control experiment using aniline **3b** as the radical clock probe.[28] Assuming that SET between **3b** and λ^3-bromane **2a** is feasible, the generated radical cation $\mathbf{3b}^{\bullet+}$ should feature aryl radical character (shown are only two resonance forms for $\mathbf{3b}^{\bullet+}$; see Eq. (4), Scheme 3). The *O*-allyl-substituted aryl radicals such as $\mathbf{3b}^{\bullet+}$ are well-known to undergo the radical 5-*exo* cyclization to $\mathbf{7}^{\bullet+}$ with an extremely high rate constant (k = 6.3×10^9 s^{-1} at 30 °C).[29] Subsequent deprotonation and hydrogen atom transfer from MeCN would furnish 2,3-dihydrobenzofurane **8**. Notably, the formation of **8** was not observed in the crude reaction mixture of the oxidative amination. Instead, the desired oxidative amination product **6b** was isolated in 63% yield (Eq. (1), Scheme 3). Finally, important evidence against the intermediacy of radical cation $\mathbf{3a}^{\bullet+}$ was obtained by EPR studies. Specifically, the formation of radicals could not be observed upon mixing λ^3-bromane **2a** (0.1 M solution in MeCN)

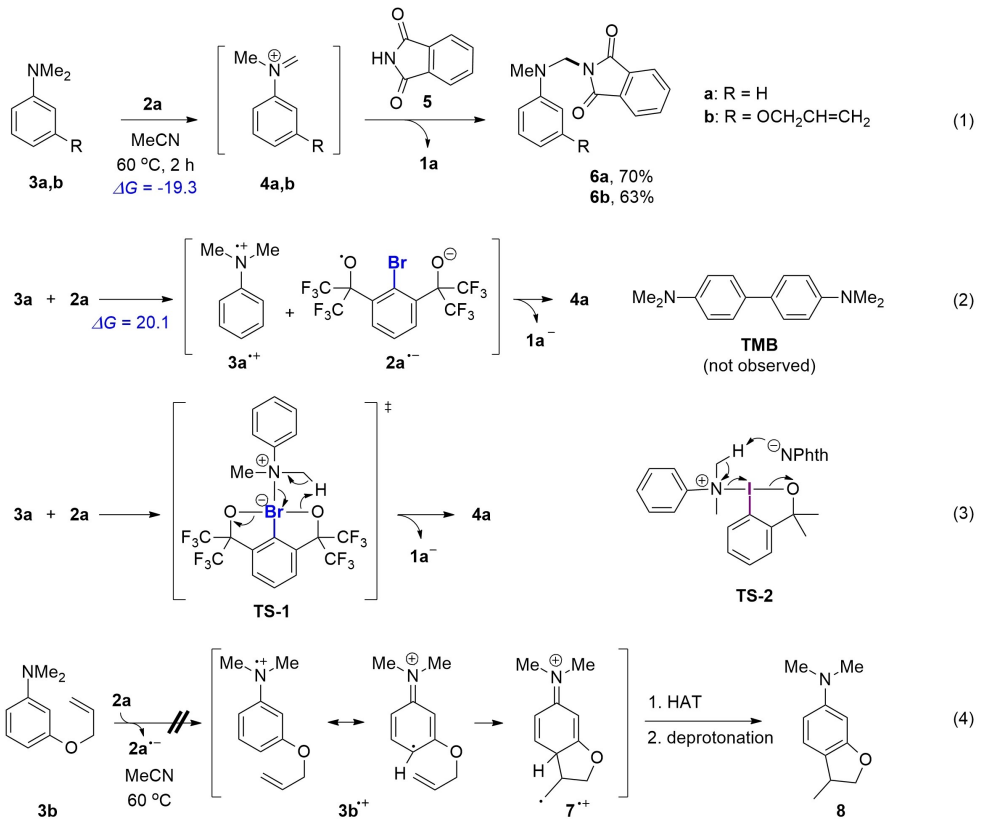

Scheme 3. Mechanistic studies of oxidative aminations induced by **2a** (calculated free energies in kcal mol^{-1}).

with aniline **3a** (0.1 M solution in MeCN) at room temperature. In striking contrast, the formation of a persistent radical intermediate from **2a** and **3a** was clearly observed when HFIP was used as the solvent at room temperature (for details see Figure S5 in the Supporting Information). Furthermore, the oxidative amination experiment in HFIP using aniline **3b** as the radical clock probe (Eq. (4), Scheme 3) returned a highly complex mixture of unidentified products. This result implies a change of the reaction mechanism upon replacing MeCN by HFIP as the solvent. Consequently, the combined mechanistic evidence suggests the SET oxidation of anilines to radical cations **3**$^{\bullet+}$ by λ^3-bromane **2a** is unlikely under the published oxidative amination conditions in MeCN as the solvent.[15] The formation of iminium ion **4a** in MeCN apparently follows an ionic pathway, involving intramolecular β-deprotonation within a transient [12-Br-4] complex **TS-1** between aniline **3a** and Lewis acidic λ^3-bromane **2a** (Eq. (3), Scheme 3). In agreement with the abundant experimental evidence, quantum chemical calculations suggest that an ionic pathway to **6a** via **4a** is thermodynamically well feasible as illustrated by Figure S8 in the Supporting Information.

Acidic bromane activation

In contrast to the efficiency of λ^3-bromane **2a** in the oxidative amination of anilines, the activation of bromine(III) reagent **2a** by the addition of Lewis or Brønsted acids was found to be necessary to accomplish the homocoupling of arenes such as **9** to biaryl **10** in CH_2Cl_2 (Eq. (1), Scheme 4).[15] Importantly, the closely related hypervalent iodine(III)-mediated oxidative biaryl coupling was shown to proceed through SET oxidation of electron-rich arenes to the corresponding cation radicals **11**$^{\bullet+}$ (Eq. (2), Scheme 4),[30] and Lewis acid additives such as $BF_3{\cdot}OEt_2$ were required to enhance the SET oxidizing ability of $PhI(OCOCF_3)_2$.[31,32] Assuming a similar mechanism for iodine(III) and bromine(III)-mediated biaryl coupling, the requirement for a Lewis acid additive to enhance the SET oxidizing ability of λ^3-bromane **2a** becomes evident given its more negative reduction potential ($E_{P/2} = -0.57$ V) compared to $PhI(OCOCF_3)_2$ ($E_{P/2} = -0.20$ V, see the Supporting Information).

TMS-OTf was chosen as Lewis acid additive for the bromine(III)-mediated biaryl coupling.[33] A nearly quantitative formation of biaryl **10** (98% yield) was observed after 3 h at −30 °C (Eq. (1), Scheme 4), when **2a** was used together with 1 equiv. TMS-OTf.[34] It should be noted that the formation of **10** was not observed with added TMS-OTf in the absence of **2a**. Importantly, TfOH as the additive (1.05 equiv) also resulted in the **2a**-mediated formation of biaryl in DCM as the solvent (93% yield of **10**). This observation led us to hypothesize that partial hydrolysis of TMSOTf by traces of water under the biaryl coupling conditions may take place to form TfOH, which is the actual activator of **2a**.[35] To verify this hypothesis, the TMSOTf-mediated biaryl coupling was performed under standard

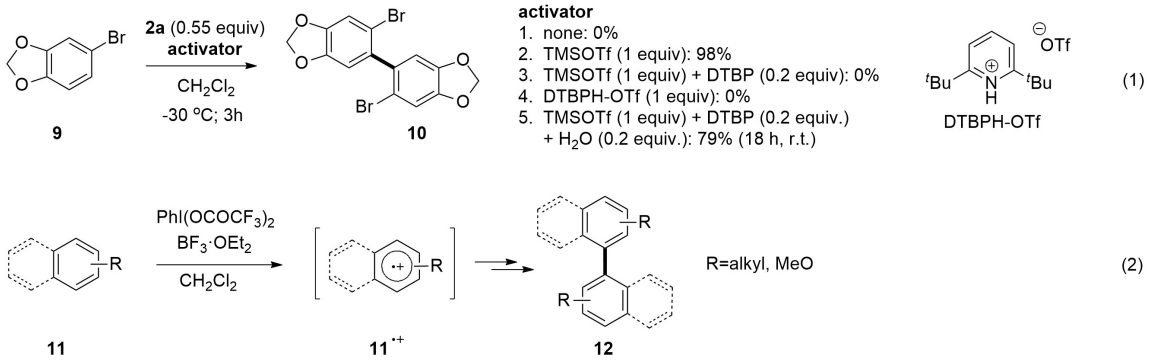

Scheme 4. Activation of **2a** for oxidative biaryl homo-coupling.

reaction conditions in the presence of sub-stoichiometric amounts of DTBP (0.2 equiv) as a proton scavenger (Eq. (1), Scheme 4). The formation of **10** was not observed with the added DTBP. Furthermore, the biaryl coupling also did not proceed in the presence of 2,6-di-*tert*-butylpyridinium triflate (1.0 equiv; prepared *in situ* from equimolar amounts of TfOH and DTBP), a relatively weak Brønsted acid that is generated upon proton quench by DTBP. However, biaryl **10** was slowly formed in 79% yield using TMSOTf (1 equiv) with added DTBP (0.2 equiv) and water (0.2 equiv) at room temperature. Possibly, a small excess of TfOH (trace amounts of the acid present in TMSOTf combined with TfOH that was formed upon hydrolysis of TMSOTf) with respect to DTBP was sufficient to catalyze the formation of biaryl **10**. Taken together, these experiments provide evidence favoring the activation of the biaryl coupling by TfOH that is generated *in situ* from TMS-OTf.

Additional support for the acid-base interactions between λ^3-bromane **2a** and Brønsted acid was obtained by NMR experiments. Thus, a downfield displacement of ^{1}H NMR signals ($\delta = 0.03$ and 0.04 ppm) and ^{19}F NMR signal ($\delta = 0.19$ ppm) for λ^3-bromane **2a** was observed upon addition of two equivalents of TfOH (see table, Figure 6B). In sharp contrast, the addition of TMSOTf (2 equiv) or $BF_3{\cdot}OEt_2$ (2 equiv) did not lead to noticeable changes in the NMR spectra of **2a**. Apparently, TMS-OTf is not a sufficiently strong Lewis acid to form a stable complex with the moderately Lewis basic oxygen atom of the bromaoxole subunit in **2a**. Overall, the experiments above provide evidence that the activation of λ^3-bromane **2a** requires protonation by a strong Brønsted acid such as TfOH (Figure 6A).

Quantum chemical calculations were performed to provide additional insights into the protonation of λ^3-bromane **2a** with TfOH. According to our results on the local coupled cluster level of theory, the protonation of **2a** to **2a–TfOH** is associated with a free reaction energy of $\triangle G = 5.8$ kcal mol^{-1} and virtually no reaction barrier (see Figure 6A; the optimized geometry of the adduct is shown in Figure 6C). This implies that only a small fraction of **2a** is protonated by added stoichiometric TfOH which agrees well with the relatively small displacements in chemical shifts observed in ^{19}F and ^{1}H NMR spectra for the 1:2 mixture of **2a**:**TfOH** (Figure 6B). In contrast, the computed ^{19}F and ^{1}H chemical shift values for **2a–TfOH** show more pronounced displacements; the calculated average displace-

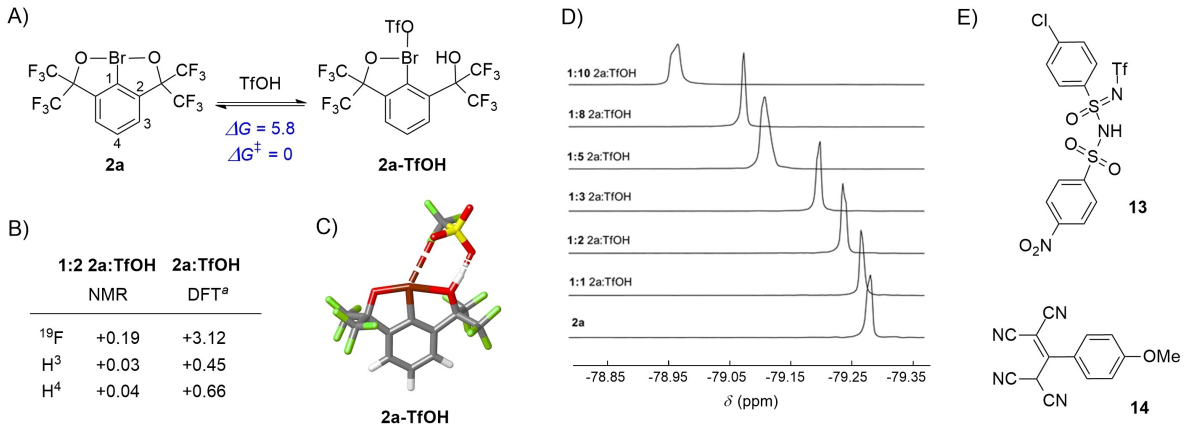

Figure 6. A) Adduct formation between TfOH and **2a** with calculated Gibbs free energy in kcal mol^{-1}. B) Comparison between the observed shifts of ^{1}H and ^{19}F signals for **2a** upon the addition of TfOH (2.0 equiv) in CD_2Cl_2 (trifluorotoluene as the internal standard) and the computed shifts. The positive signs refer to downfield displacements. [a] Averaged chemical shifts. C) Computed optimized geometry of **2a**-**TfOH**. D) Displacement of ^{19}F chemical shifts for **2a** in the presence of various amounts of TfOH. E) Reference compounds for titration experiments.

ment value for chemical shifts of the two protons at position 3 amounts to $\delta = 0.45$ ppm when going from **2a** to **2a**-**TfOH**, while that for a proton at position 4 amounts to 0.66 ppm. Furthermore, an average shift of $\delta = 3.12$ ppm is predicted for the ^{19}F signals. When compared with the observed displacements of the ^{1}H and ^{19}F NMR shifts for a 1:2 mixture of **2a**:**TfOH**, the computed values have the correct sign and roughly the correct relative size. Therefore, taking into account the small fraction of formed **2a**-**TfOH** under these conditions and considering the progression of the signal position for higher acid concentrations shown in Figure 6D, the computed NMR shifts agree well with our experimental observations and thus support the proposed mechanistic picture of equilibrium protonation of **2a** by the added TfOH. These findings, together with the absence of any displacement of the NMR shifts for a 1:2 mixture of **2a**:**TMSOTf**, provide further evidence for the indirect role of **TMSOTf** in terms of activating **2**.

The observed equilibrium protonation of λ^3-bromane **2a** called for additional experiments to estimate the approximate acidity of the solution needed for protonating **2a**, in terms of the unified pH ($pH_{abs}^{H_2O}$) scale.[36] The term "$pH_{abs}^{H_2O}$" stands for unified pH (pH_{abs}) "aligned" with the aqueous pH scale, that is, the $pH_{abs}^{H_2O}$ values in any solvent are directly comparable with the conventional aqueous pH values. In other words, in a solution with a given $pH_{abs}^{H_2O}$, made in any solvent, the chemical potential of the solvated proton is equal to the chemical potential of solvated proton in water at the same value of conventional pH.[37]

The acidity necessary for protonation of **2a** is expressed as "buffer point $pH_{abs}^{H_2O}$ ", that is, $pH_{abs}^{H_2O}$, at which approximately half of **2a** is free and half has TfOH added (**2a**-**TfOH**, Figure 6A). Experiments for determination of the buffer point were carried out in 1,2-dichloroethane, where a self-consistent acidity scale has been previously established and linked to the unified pH ($pH_{abs}^{H_2O}$) scale.[38] The experiments consisted in titration of a mixture of **2a** and a reference compound, for which the pK_a and buffer point $pH_{abs}^{H_2O}$ estimates are available in 1,2-dichloroethane.[38] Different reference compounds were tried. The titration experiments gave a clearly interpretable outcome only with **13** (monitored by ^{19}F NMR) and **14** (monitored by UV-Vis spectrometry; see Figure 6E and the Supporting Information). The obtained buffer points are as follows: the buffer point $pH_{abs}^{H_2O}$ from titration of **13** was −6.8 and from titration of **14** was −8.5. Thus, the average value of the buffer point $pH_{abs}^{H_2O}$, together with an uncertainty estimate would be (-7.7 ± 1.2). This value has high uncertainty but allows qualitative interpretation: it means that by its acidity, in terms of the chemical potential of the solvated proton, such solution corresponds approximately to a hypothetical aqueous solution with pH −7.7. The uncertainty estimate embraces the full range of variability that we have seen in our experiments. Additional explanations, descriptions of experiments, and the obtained NMR and UV-Vis spectra are presented in the Supporting Information.

Conclusion

A combination of experimental and quantum chemical methods provided important insight into electrochemical properties and reactivity of chelation-stabilized λ^3-bromanes. Cyclic voltammetry studies in HFIP show that the anodic oxidation of parent bromoarenes that are equipped with coordinating hexafluoro-2-hydroxy-propanyl units in positions 2 and 6 proceeds via parallel ECEC and ECE_{disp} sequences, whereby the initially formed cation radical intermediate could be detected in the case of the *para*-methoxy-substituted bromoarene by UV-Vis spectroelectrochemistry. In contrast, cathodic conversion of the chelation-stabilized λ^3-bromanes to parent bromoarenes in acetonitrile occurs via single electron reduction, followed by hydrogen atom abstraction from the solvent and protonation. The corresponding half-peak potentials indicate that Martin's-type λ^3-bromanes are rather poor single electron oxidants. This important finding was corroborated by mechanistic studies of bromine(III)-mediated oxidative amidation of *N*,*N*-dimethylanilines in MeCN that provided compelling evidence against the involvement of a SET mechanism. The oxidative amidation in MeCN apparently proceeds through an ionic mechanism, involving an inner-sphere redox process within a transient [12-Br-4] complex. On the other hand, chelation-stabilized λ^3-bromanes possess comparable SET oxidizing ability to that of hypervalent iodine(III) reagents such as PIFA. The latter requires activation by Lewis acid to effect SET oxidation in, for example, oxidative biaryl coupling, whereas the activation by a strong Brønsted acid such as TfOH turned out to be the most efficient for Martin's-type λ^3-bromanes. The observed displacements of chemical shifts in ^{1}H and ^{19}F NMR spectra for λ^3-bromane suggests its equilibrium protonation by the added TfOH with a buffer point $pH_{abs}^{H_2O}$ determined to be -7.7 ± 1.2 by titration experiments in 1,2-dichloroethane. The protonation presumably leads to the cleavage of benzabromooxole ring and the formation of more reactive bromonium(III) triflate that features enhanced $[Ar{-}Br]^+$ cationic character as reflected by a LUMO energy reduction of 1.01 eV and a slight increase of the Mulliken charge population by 0.07 units and, hence, increased Lewis acidity and oxidizing ability.[32] Overall, we believe that the detailed mechanistic understanding of electrochemical properties and reactivity of the chelation-stabilized λ^3-bromanes will help to widen the use of hypervalent bromine(III) species in contemporary organic synthesis and accelerate the development of unprecedented synthetic transformations. Our ongoing work on the electrochemical synthesis of various bromine(III) species and their application in organic synthesis will be reported in due course.

Acknowledgements

This work was funded by the German Research Foundation (DFG, Grant No. FR 3848/1-2 and RO 5688/1-1), ERDF (Post-Doc Latvia) project No. 1.1.1.2/VIAA/2/18/377, by the EMPIR program (project 17FUN09 "UnipHied", www.uniphied.eu) co-financed by the Participating States and from the European Union's Horizon

2020 research and innovation program and by the Estonian Research Council grant (PRG690). R.F. is grateful for financial support by the DFG (Heisenberg Program, Grant No. FR 3848/4-1). The authors thank Dr. Larisa Baumane (Latvian Institute of Organic Synthesis) for EPR experiments. Open Access funding enabled and organized by Projekt DEAL.

Conflict of Interest

The authors declare no conflict of interest.

Data Availability Statement

The data that support the findings of this study are available in the supplementary material of this article.

Keywords: hypervalent halogen · bromane · oxidative coupling · cyclic voltammetry · unified pH

[1] a) T. Wirth (Ed.) *Top. Curr. Chem., Vol. 373*, Springer, **2016**; b) I. Marek (Ed.) *Patai's Chemistry of Functional Groups*, John Wiley & Sons, Hoboken, **2018**; c) A. Yoshimura, V. V. Zhdankin, *Chem. Rev.* **2016**, *116*, 3328; d) R. Francke, *Curr. Opin. Electrochem.* **2021**, *28*, 100719; e) M. Elsherbini, T. Wirth, *Chem. Eur. J.* **2018**, *24*, 13399; f) R. Francke, *Curr. Opin. Electrochem.* **2019**, *15*, 83.
[2] U. Farooq, A.-U.-H. A. Shah, T. Wirth, *Angew. Chem. Int. Ed.* **2009**, *48*, 1018.
[3] K. Miyamoto in *Patai's Chemistry of Functional Groups* (Ed.: I. Marek), John Wiley & Sons, Hoboken, **2018**, DOI: 10.1002/9780470682531.pat0956.
[4] B. Winterson, T. Patra, T. Wirth, *Synthesis* **2022**, *54*, 1261.
[5] M. Ochiai, A. Yoshimura, T. Mori, Y. Nishi, M. Hirobe, *J. Am. Chem. Soc.* **2008**, *130*, 3742.
[6] M. Ochiai, T. Okada, N. Tada, A. Yoshimura, K. Miyamoto, M. Shiro, *J. Am. Chem. Soc.* **2009**, *131*, 8392.
[7] M. Ochiai, K. Miyamoto, T. Kaneaki, S. Hayashi, W. Nakanishi, *Science* **2011**, *332*, 448.
[8] a) K. Miyamoto, M. Saito, S. Tsuji, T. Takagi, M. Shiro, M. Uchiyama, M. Ochiai, *J. Am. Chem. Soc.* **2021**, *143*, 9327; b) Md. M. Hoque, K. Miyamoto, N. Tada, M. Shiro, M. Ochiai, *Org. Lett.* **2011**, *13*, 5428; c) M. Ochiai, T. Kaneaki, N. Tada, K. Miyamoto, H. Chuman, M. Shiro, S. Hayashi, W. Nakanishi, *J. Am. Chem. Soc.* **2007**, *129*, 12938; d) M. Ochiai, Y. Nishi, S. Goto, M. Shiro, H. Frohn, *J. Am. Chem. Soc.* **2003**, *125*, 15304; e) H. J. Frohn, M. Giesen, *J. Fluorine Chem.* **1998**, *89*, 59.
[9] M. Ochiai, A. Yoshimura, K. Miyamoto, S. Hayashi, W. Nakanishi, *J. Am. Chem. Soc.* **2010**, *132*, 9236.
[10] Y. Yoshida, S. Ishikawa, T. Mino, M. Sakamoto, *Chem. Commun.* **2021**, *57*, 2519.
[11] M. Lanzi, R. A. Ali Abdine, M. de Abreu, J. Wencel-Delord, *Org. Lett.* **2021**, *23*, 9047.
[12] a) T. T. Nguyen, J. C. Martin, *J. Am. Chem. Soc.* **1980**, *102*, 7382; b) T. T. Nguyen, S. R. Wilson, J. C. Martin, *J. Am. Chem. Soc.* **1986**, *108*, 3803.
[13] a) T. Broese, R. Francke, *Org. Lett.* **2016**, *18*, 5896; b) W.-C. Gao, Z.-Y. Xiong, S. Pirhaghani, T. Wirth, *Synthesis* **2019**, *51*, 276; c) A. F. Roesel, T. Broese, M. Májek, R. Francke, *ChemElectroChem* **2019**, *6*, 4229–4237; d) M. Elsherbini, B. Winterson, H. Alharbi, A. A. Folgueiras-Amador, C. Génot, T. Wirth, *Angew. Chem. Int. Ed.* **2019**, *58*, 9811; e) A. Maity, B. L. Frey, N. D. Hoskinson, D. C. Powers, *J. Am. Chem. Soc.* **2020**, *142*, 11, 4990; f) J. D. Herszman, M. Berger, S. R. Waldvogel, *Org. Lett.* **2019**, *21*, 7893; g) S. Doobary, A. T. Sedikides, H. P. Caldora, D. L. Poole, A. J. J. Lennox, *Angew. Chem. Int. Ed.* **2020**, *59*, 1155; h) B. Devadas, J. Svoboda, M. Krupička, T. Bystron, *Electrochim. Acta* **2020**, *342*, 136080.
[14] O. Koleda, T. Broese, J. Noetzel, M. Roemelt, E. Suna, R. Francke, *J. Org. Chem.* **2017**, *82*, 11669.
[15] I. Sokolovs, N. Mohebbati, R. Francke, E. Suna, *Angew. Chem. Int. Ed.* **2021**, *60*, 15832.
[16] V. V. Pavlishchuk, A. W. Addison, *Inorg. Chim. Acta* **2000**, *298*, 97.
[17] J. Heinze, *Angew. Chem. Int. Ed. Engl.* **1984**, *23*, 831.
[18] R. F. Nelson, *J. Electroanal. Chem.* **1968**, *18*, 329.
[19] C. Hansch, A. Leo, R. W. Taft, *Chem. Rev.* **1991**, *91*, 165.
[20] F. M'Halla, J. Pinson, J. M. Saveant, *J. Am. Chem. Soc.* **1980**, *102*, 4120.
[21] E. Oberem, A. F. Roesel, A. Rosas-Hernández, T. Kull, S. Fischer, A. Spannenberg, H. Junge, M. Beller, R. Ludwig, M. Roemelt, R. Francke, *Organometallics* **2019**, *38*, 1236.
[22] D. Zhu, Y. Yao, R. Zhao, Y. Liu, L. Shi, *Chem. Eur. J.* **2018**, *24*, 4805.
[23] N. Döben, H. Yan, M. Kischkewitz, J. Mao, A. Studer, *Org. Lett.* **2018**, *20*, 7933.
[24] K. Kiyokawa, T. Kosaka, T. Kojima, S. Minakata, *Angew. Chem. Int. Ed.* **2015**, *54*, 13719.
[25] T. A. Brown, H. Chen, R. N. Zare, *Angew. Chem. Int. Ed.* **2015**, *54*, 11183.
[26] F. Cao, J. Kim, A. J. Bard, *J. Am. Chem. Soc.* **2014**, *136*, 18163.
[27] The major product identified in the reaction mixture was *N*-methylaniline that was presumably formed from iminium ion **4a** upon aqueous workup.
[28] D. Griller, K. U. Ingold, *Acc. Chem. Res.* **1980**, *13*, 317.
[29] L. J. Johnston, J. Lusztyk, D. D. M. Wayner, A. N. Abeywickreyma, A. L. J. Beckwith, J. C. Scaiano, K. U. Ingold, *J. Am. Chem. Soc.* **1985**, *107*, 4594.
[30] Y. Kita, K. Morimoto, M. Ito, C. Ogawa, A. Goto, T. Dohi, *J. Am. Chem. Soc.* **2009**, *131*, 1668.
[31] T. Dohi, M. Ito, N. Yamaoka, K. Morimoto, H. Fujioka, Y. Kita, *Tetrahedron* **2009**, *65*, 10797.
[32] S. Izquierdo, S. Essafi, I. Del Rosal, P. Vidossich, R. Pleixats, A. Vallribera, G. Ujaque, A. Lledós, A. Shafir, *J. Am. Chem. Soc.* **2016**, *138*, 12747.
[33] V. V. Zhdankin, A. Y. Koposov, L. Su, V. V. Boyarskikh, B. C. Netzel, V. G. Young, *Org. Lett.* **2003**, *5*, 1583.
[34] Alternatively, $BF_3{\cdot}OEt_2$ could be used for the activation of bromane **2a** in HFIP as the solvent (35% yield of **10**).
[35] Y.-B. Kang, L. H. Gade, *J. Am. Chem. Soc.* **2011**, *133*, 3658.
[36] a) D. Himmel, S. K. Goll, I. Leito, I. Krossing, *Angew. Chem. Int. Ed.* **2010**, *49*, 6885; b) A. Suu, L. Jalukse, J. Liigand, A. Kruve, D. Himmel, I. Krossing, M. Rosés, I. Leito, *Anal. Chem.* **2015**, *87*, 2623.
[37] V. Radtke, D. Stoica, I. Leito, F. Camões, I. Krossing, B. Anes, M. Roziková, L. Deleebeeck, S. Veltzé, T. Näykki et al., *Pure Appl. Chem.* **2021**, *93*, 1049.
[38] E. Paenurk, K. Kaupmees, D. Himmel, A. Kütt, I. Kaljurand, I. A. Koppel, I. Krossing, I. Leito, *Chem. Sci.* **2017**, *8*, 6964.

Manuscript received: March 29, 2022
Accepted manuscript online: May 5, 2022
Version of record online: June 10, 2022